Electrochimica Acta 457 (2023) 142510

Contents lists available at ScienceDirect

Electrochimica Acta

journal homepage: www.journals.elsevier.com/electrochimica-acta

Influence of pH and temperature in the performance of Zn phosphate conversion coatings

Sheila Silva-Fernández, Belén Díaz *, Iria Feijoo, Xosé Ramón Nóvoa, Carmen Pérez

CINTECX, Universidade de Vigo, EEI, ENCOMAT Group, Vigo 36310, Spain

ARTICLE INFO

Keywords:
Phosphate conversion coating
Ph
Temperature
Corrosion resistance
Microstructure
Impedance spectroscopy

ABSTRACT

The influence of variations in temperature (from 50 °C to 70 °C) and pH (2.4 and 2.9) in the Zn phosphate conversion treatment of a high-strength steel was assessed in this study. The effect of the temperature changes depends on the pH of the bath. The results evidenced an enhanced corrosion resistance with the increased temperature for baths at pH 2.4, whereas no relevant differences were concluded for baths at pH 2.9. This latter pH condition provided a better surface coverage, even with lower coating masses, than the former value. The microstructural analysis showed the development of films composed of smaller crystals for the treatments at pH 2.9. Impedance spectroscopy was established as a powerful tool with great potential for characterising phosphate layers. The accuracy of this methodology greatly depends on the equivalent circuit used for the simulation. A model based on the transmission line allows the reliable estimation of the percentage of exposed area (coating efficiency), the identification of changes in the film conductivity, and the qualitative analysis of its structure.

1. Introduction

The attractiveness of phosphate technology lies in its wide range of applications. The phosphate films increase the corrosion resistance, improve the adhesion of organic paints deposited on them and enhance the wear resistance. It can also be applied on various metals, plain carbon steel, galvanized steel, stainless steel, Mg or Al, among others, by a relatively simple, fast, and low-cost process. Other coating techniques in some applications have indeed substituted it since the phosphating process has some disadvantages, the formation of sludges that reduce the bath lifetime and the requirement of careful control in the experimental parameters are the most remarkable. However, it is still an essential practice as a base coating in car manufacturing in many countries or as a lubricant in cold-forming operations. Several studies have also reflected the improved corrosion performance of phosphated reinforcing concrete bars with the resulting increase in the bond strength at the bar/concrete interface [1–3]. Furthermore, zinc phosphate is suitable for modifying the surface of biomaterials and its application is gaining relevance in this field [4].

Many attempts to enhance the performance of phosphate films have been recorded over the past decades. However, some most recent efforts focus on adjusting the phosphate solution's chemistry. Furthermore, some eco-friendly additives are being assessed due to the current industrial requirement that urges the removal of harmful substances, such as certain metal cations. Thus, incorporating nano SiO_2, TiO_2, graphene oxide, or polyvinyl alcohol is among the most innovative strategies [5–13]. However, this kind of modification could imply an increase in the cost of the treatment.

The present study aims to optimise the phosphating process, but focusing on traditional baths, and elucidates the importance of two parameters, pH and temperature. Their effect on the structure and performance of the obtained films will be assessed. The careful definition of the bath pH and temperature can be a simple and cost-effective strategy for a successful solution.

Several authors have already focused on assessing pH and temperature changes in the phosphate treatments. However, no clear conclusions could be deduced from these studies. An improved corrosion response was usually found due to the increase in temperature [2, 14–17], whereas modifications in pH typically reflect a more significant variability in the characteristics of the films [7,18–20]. The chemical knowledge behind the phosphate technology is relatively complex, and other factors, such as the composition of the solution, type of metal, accelerators or time, have been identified as modifiers in the whole process [21]. This means that the obtained conclusions concerning the effect of any modification in the experimental routine should be exclusively applied to the conditions where that research was performed,

* Corresponding author.
E-mail address: belenchi@uvigo.es (B. Díaz).

https://doi.org/10.1016/j.electacta.2023.142510
Received 17 January 2023; Received in revised form 24 April 2023; Accepted 1 May 2023
Available online 2 May 2023

being inaccurate to use for other treatments. Thus, each treatment with its specific variables should be analysed to investigate the role of either pH or temperature properly.

From a general perspective, pH modifies the phosphoric acid dissociation equilibrium (Eq. (1)), resulting in decreased free phosphoric acid in a higher pH bath. The amount of phosphoric acid must be carefully controlled since it is responsible for the attack of the metal surface that initiates the formation of the phosphate layer [21]. Concerning the temperature, its main effect, as well as the acceleration in the kinetics of the process, is the assistance for transforming the soluble phosphates into the intended insoluble products [22].

$$H_3PO_4 \rightarrow^{\leftarrow} H_2PO_4^- + H^+ \quad (1)$$

The reliability of the discussions offered in the literature also depends on the methodology used to characterise the phosphate coatings. The most common analytical techniques for evaluating the quality of the formed films are X-Ray Diffraction (XRD) and Scanning Electron Microscopy (SEM), which give transparent and undoubted information on the structure, composition, and morphology. However, to provide a complete or "macroscopic" evaluation, particularly from the coverage ability point of view, other less localised methods as the electrochemical techniques, are usually applied. The polarisation procedure is very commonly used since it allows the fast and easy determination of corrosion resistance. This result is generally supported with impedance spectroscopy, from which, for most of the publications, the provided information is also limited to the corrosion performance. We will show here that this methodology can be used as a complementary technique to give other essential knowledge related to phosphate film features.

2. Experimental

2.1. Materials and chemical conversion process

Hot-rolled high-strength steel rods with the composition given in Table 1 were used in this study. Before the phosphating, samples were degreased in 0.1 M NaOH for 5 min and pickled in 2 M H_2SO_4 at 50 °C for 20 min. After rinsing in water, the activation process was followed by soaking in a titanium phosphate colloidal aqueous solution (1 g/L) at room temperature for 2 min. This step aims to accelerate the chemical conversion process and assist in developing a finer structure with better coverage [23].

The samples were then treated in the phosphating bath described in Table 2, which includes a conventional mixture of nitrates and nitrites as accelerators, for 6 minutes, at temperatures of 50 °C, 60 °C and 70 °C. Treatments were followed at two different pH values, 2.4 ± 0.1, the natural pH of the prepared solution, and 2.9 ± 0.1, a bigger pH to assess the effect of this variable, which was adjusted by adding 1 MNaOH. No further pH increments were tested to avoid an excessive sludge formation, as already found in the literature [15,24]. After the chemical conversion process, samples were rinsed in water, dried with warm air, and kept in a desiccator before the film characterization.

2.2. Phosphate conversion coating characterisation

The coating structure and morphology were studied with a Scanning Electron Microscope, a JEOL® 5410 from OXFORD. In addition, the secondary electron images were taken with an accelerating voltage of 20 kV and at a working distance of 10 mm. The microscope was equipped with an Energy Dispersive Spectrometer detector, a Link ISIS 300 EDS, which allowed the chemical characterization of the phosphate films.

Table 2
Composition of the phosphating bath.

H_3PO_4	ZnO	$NaNO_3$	$NaNO_2$
13.1 g/L	3.5 g/L	3 g/L	0.1 g/L

The coating weights (mass per unit area, g/m^2) were measured by the stripping method, using a solution with 12% Na_4EDTA, 9% NaOH and 4% TEA at 70 °C for 5 min. The weight of the specimens was measured before and after stripping, and the mass loss was then referred to per unit area of the substrate.

The classical three-electrode cell was used for the electrochemical characterisation with a $Hg/HgSO_4$ and a graphite sheet as reference and auxiliary electrodes, respectively. The testing electrolyte was a 0.1 MNa_2SO_4 solution. The tests were performed in an AUTOLAB PGSTAT-204 potentiostat from Metrohm. The corrosion resistance was measured with the potentiodynamic polarisation technique, where potential values from −150 mV to +150 mV, with respect to the Open Circuit Potential (OCP), were swept at 1 mV/second. The corrosion current density (i_{corr}) was determined after a Tafel analysis. The percentage of the uncovered area (UA,%) was obtained by comparison with the corresponding value of the pickled substrate, according to Eq. (2). The current density value is proportional to the area that remains exposed to the electrolyte so that the lowest the current density, the lowest the uncovered area and the greatest the coating efficiency.

$$UA(\%) = \frac{i_{corr-phosphated\ sample}}{i_{corr-pickled\ sample}} x100 \quad (2)$$

Electrochemical Impedance Spectroscopy (EIS) measurements at the OCP were also done. The spectra in the frequency range between 100 kHz and 10 mHz were recorded using a potential signal amplitude of 10 mV rms.

The impedance spectra were fitted to obtain quantitative information using the equivalent circuits presented in Fig. 1. Fig. 1a shows a circuit commonly used for the simulation of surfaces that are covered with phosphate films. The time constant at the high frequency (C_{film} and R_{film}) gives information about the own phosphate layer. In contrast, the low-frequency element (C_{dl} and R_{ct}) is related to the corrosion response of the uncoated metal surface. The equivalent model indicated in Fig. 1b was also used. It corresponds to a transmission line (TL) that considers the phosphate conversion film as a porous electrode [25], where the current is not uniformly distributed on the electrode [26]. It consists of two parts. One part is related to the metal surface, i.e., to the electrolyte/metal interface at those uncoated areas, represented by the Z_2 element. The other part corresponds to the porous material with a total L length. This length value must be fixed to perform the simulation, so the numerical value computed from the coating mass divided by the film density was used [21]. The R_m and R_s parameters are distributed along the length of the film (L) and describe the resistance of the electrode material and the electrolyte inside the pores, respectively. Z_1 represents the electrode/electrolyte interface at the walls of the pores and is distributed along the film. Z_1 and Z_2 are composed of a parallel combination of resistance and capacitance. True capacitances have been considered for the impedance analysis to provide a physical explanation for the obtained values. The time-constants distribution was allowed by the integration of dispersion parameters, as conventionally done by the authors [27].

Table 1
Composition of the metal substrate used in this study (weight%).

C	Mn	Si	S	P	Cr	Ni	Mo	Cu	V	N	Fe
0.815	0.783	0.160	0.003	0.007	0.150	0.070	0.013	0.116	0.004	0.007	balance

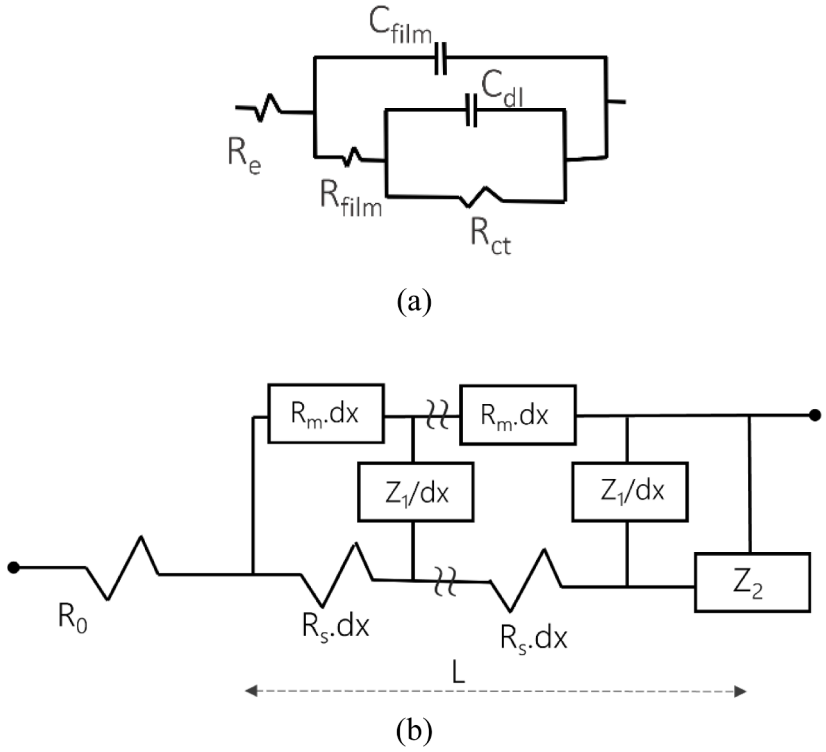

Fig. 1. Equivalent circuits used for the fitting of the impedance measurements. See the text for details.

3. Results and discussion

3.1. Microstructural characterisation: SEM and EDX

The SEM images presented in Fig. 2 correspond to the films obtained in this study. From the morphological point of view, a noticeable difference exists as a function of the pH used in the phosphating bath. Independently on the temperature, an important crystal size refinement can be identified if the phosphating bath is alkalinized from 2.4 up to 2.9, in agreement with other studies [15]. among the films grown in the most acidic solution, a variation in the covering efficiency is evident since some uncoated areas can be evidenced for those layers developed at 50 °C and 60 °C. However, with the increase in temperature, up to 70 °C, the phosphate film shows a more compact structure that can be assigned to an acceleration in the coating rate development [15].

At pH 2.4, the bath temperature affects the type of crystals that are developed. Large prismatic crystals, with size 10–50 μm, as well as smaller cubic crystals (<10 μm), can be observed at 50 °C and 60 °C but not at 70 °C. A more uniform layer, composed of coarse crystals, can be discerned in the piece treated at this highest temperature. The chemical analysis by EDX, as compiled in Table 3, indicates a difference in composition between these two types of crystals, having a lower average Zn/Fe ratio, 1.02 vs 1.99, in those areas covered with the smaller crystals. These crystals enriched in Fe correspond to the nuclei initially created in a chemical conversion process. Once growing, they will become enriched in Zn (as found in those coarser crystals), with a higher amount of this element as the distance from the surface increases. Then, at pH 2.4, temperature plays a critical role. Many crystals can nucleate in the lowest temperature conditions, but only a few can grow. When the temperature increases to 70 °C, by contrary, the growth stage is assisted.

The influence of the treatment temperature is less relevant among those films prepared at pH 2.9. The appearance of the films is analogous, independent of the temperature, showing the presence of tiny crystals (≈ 5 μm) with a uniform covering efficiency. For this pH condition, crystals cannot grow significantly, and the phosphating process seems to be dominated by the nucleation step. Under a less aggressive phosphating solution, due to the reduction in the [H^+] ions, the coating process is initiated in many sites so that many nuclei appear. After some time, once the surface is full of nuclei, there is a constraint for further growth. As a result, the development of the crystals cannot progress since the accessibility of the electrolyte to the metal surface is limited. According to the chemical composition compiled in Table 3, these layers provide a decreased Zn/Fe ratio, around 0.6 for the three tested temperatures, lower than the value obtained in the more acidic baths (≈1, at 60 and 70 °C). It is worth to mention that the Fe content obtained from the general EDX analysis of the film obtained at 50 °C pH 2.4 is bigger due to the detection of this element coming from the uncoated spaces. The crystals formed in the less acidic bath were unable to develop, remained short, and hence higher Fe content was detected. Due to the pickling, the enriched content of Fe in the vicinity of the surface metal allows the incorporation of this specie into the conversion coating since crystals are still very close to the metal surface.

3.2. Phosphate conversion coatings: mass and covering efficiency

Table 4 shows the combined influence of the phosphating parameters, pH and temperature in the coating masses. High-temperature baths help to the creation of thicker films [2,15,17]. The coating masses increase for the layers developed at 60 °C and 70 °C, with more remarkable changes for the most acidic condition. among the three tested temperature conditions, a low pH solution assists in the development of a thicker film [17,19]. Differences are less notable for the lower temperature phosphating bath, but an increase of about 30% was measured in the mass whether the pH decreases from 2.9 to 2.4, both at 60 °C and 70 °C. This result agrees with the above discussion regarding the importance of the nucleation over the growth identified at the highest pH condition, where the thinner films are obtained. among the treatments performed at pH 2.4, it seems that above a specific temperature, around 60 °C, no significant changes are identified regarding of the masses. However, for the baths at pH 2.9, the increase in temperature assists in a more modest growth of the phosphate layer.

The polarisation curves obtained for the films prepared at the

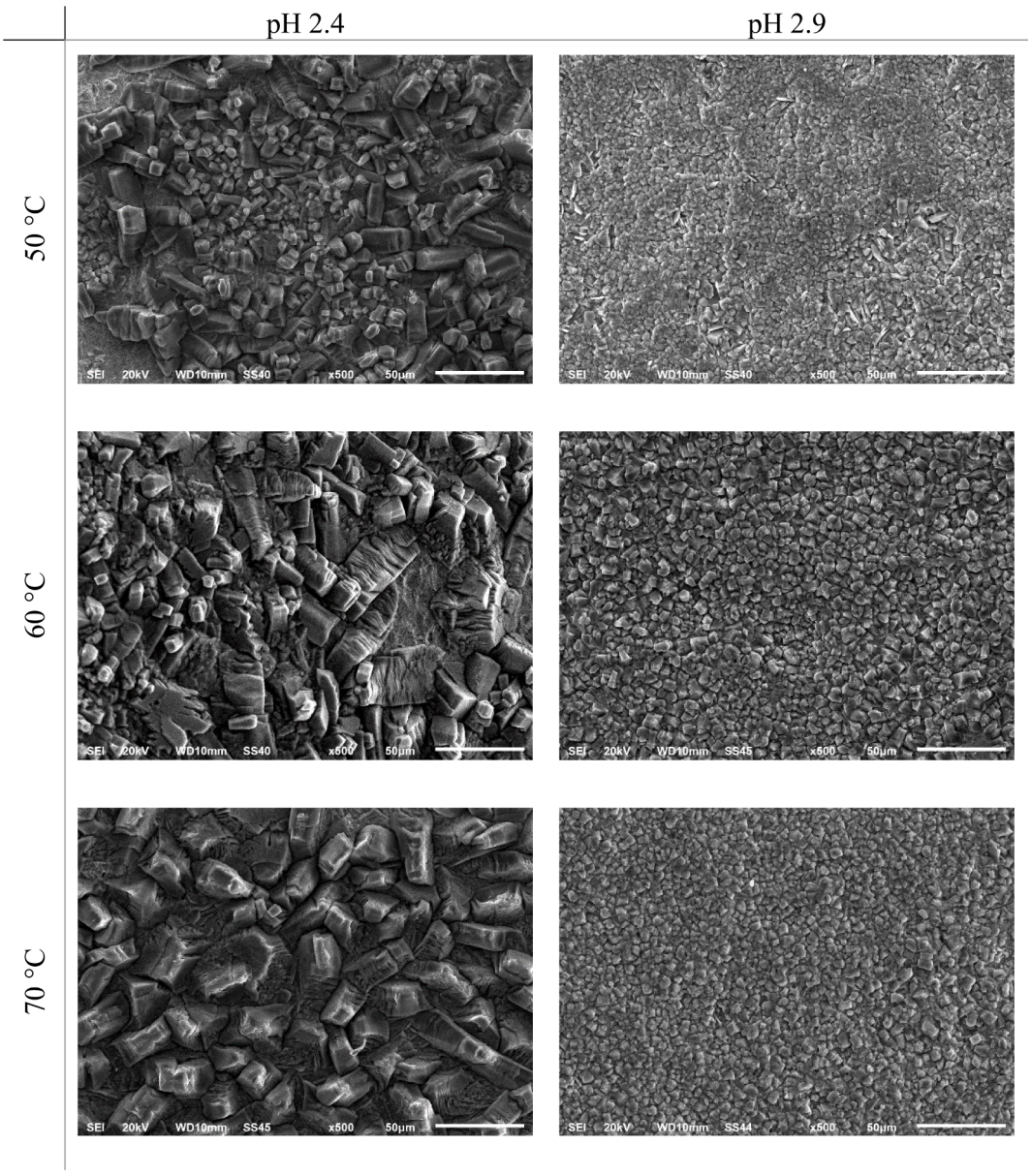

Fig. 2. SEM images of the phosphate films obtained at the indicated temperature and pH.

Table 3
Chemical composition (atomic%) obtained from the EDX analyses of the SEM images presented in Fig. 2. Note: the general analysis refers to the whole scan of the SEM image (x500), whereas the point analysis was used to examine the specific composition of the smaller or bigger crystals.

	pH	EDX analysis	Zn	P	Fe
50 °C	2.4	Smaller crystals	32.4	35.8	31.8
		Bigger crystals	36.6	45.0	18.4
		General	30.4	28.4	41.2
	2.9	General	25.8	28.7	45.5
60 °C	2.4	General	35.4	33.4	31.2
	2.9		25.4	28.9	45.7
70 °C	2.4		34.0	32.6	33.5
	2.9		27.0	30.1	42.9

specified temperatures and pH conditions are presented in Fig. 3. The corrosion resistance improvement for the layers prepared with the bath of 2.9, independent of temperature, is evident [7,15,18]. The corrosion current density (i_{corr}) values were determined, and the corresponding coating efficiencies, expressed as the percentage of area that remains exposed to the electrolyte, were computed according to Eq. (2). The obtained results are also indicated in Table 4.

Table 4
Coating masses and current density values (obtained from the polarization curves presented in Fig. 3) of the phosphate conversion coatings. The uncovered area percentages were computed following Eq. (2).

	Bare substrate	pH 2.4 50 °C	pH 2.4 60 °C	pH 2.4 70 °C	pH 2.9 50 °C	pH 2.9 60 °C	pH 2.9 70 °C
Coating mass (g/m^2)	—	7.4	9.4	9.9	6.8	7.2	7.7
i_{corr} ($\mu A/cm^2$)	6.4	23	8.9	1.7	2.2	1	1
Uncovered area (%)	—	>100	>100	26.6	34.4	15.6	15.6

A significant reduction can be verified regarding the i_{corr} for those films produced at pH 2.9. However, no significant variations were revealed according to the temperature condition, particularly above 60 °C at this pH. On the other hand, for those layers prepared at 50 °C

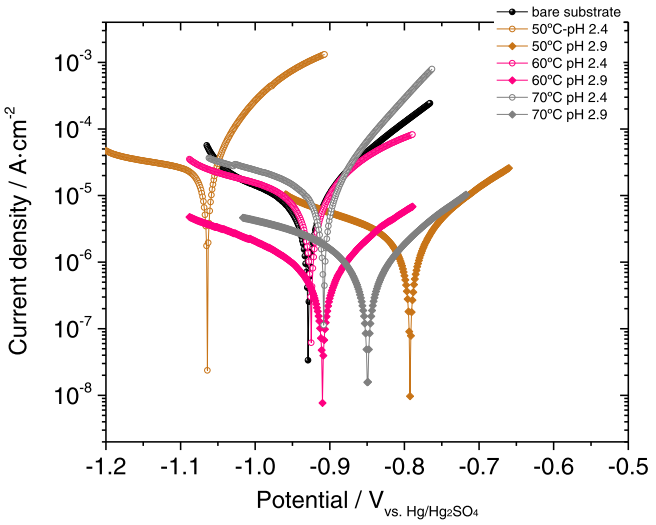

Fig. 3. Polarization curves, recorded in 0.1 M Na_2SO_4 solution, of the phosphate films prepared at several temperatures and pH.

and 60 °C, at pH 2.4, the current density values were higher than for the blank surface, as also observed in [28], and then the percentage of the uncovered area is above 100%. This result is quite surprising since, as shown in Fig. 2, the presence of the phosphate layer was evidenced even for these more acidic conditions. These abnormally high values could be explained by considering the development process of a phosphate conversion coating. One step in the coating process consists of the steel pickling due to the phosphoric acid action, resulting in this reaction producing a rougher surface. Thus, at those sites that remain uncoated after the conversion treatment, an increase in the active surface can be expected due to the increment in the roughness. The point is that, under certain phosphating conditions, the portion of the surface coated by the phosphate crystals does not compensate for the portion of the additional surface created by the phosphoric acid pickling. As pointed out in [15], there are two competing processes, the phosphate growth and the pickling reaction. The first process covers the surface with crystals whereas the other creates a rougher surface. For the lowest temperature values, at pH 2.4, the pickling dominates the process, so a very high current density value is still recorded after the phosphating treatment. However, at 70 °C, the phosphate layer development becomes faster, being able to cover, after the same period, a higher amount of surface metal. Therefore, the phosphoric acid concentration used in the phosphate bath seems more convenient for treatments at temperatures around 70 °C [23]. The bath is likely too aggressive for operations at lower temperatures, so the insoluble phosphate formation is not rapid enough.

An improvement in the corrosion performance is obtained when the pH of the phosphate bath increases to 2.9. A reduction in the current density, as indicated in Table 4, results in any of the tested temperatures. Then, the development of denser films is verified at the highest pH level. A correlation between the formation of finer crystals and improved corrosion resistance was referred to before [15].

3.3. Electrochemical impedance spectroscopy measurements

The impedance spectra obtained for the phosphate films prepared at pH 2.4 are presented in Fig. 4a. An increased resistance is obtained for the layer prepared at 70 °C. At pH 2.9, in Fig. 4b, differences are less relevant, although the coating obtained at 50 °C shows a slightly lower resistance. Comparing both plots allows for deducing an improved performance for the layers developed at the highest pH [17], at any of the tested temperatures.

For a first approach, these spectra were fitted with a simple equivalent circuit composed of two time constants (as presented in Fig. 1(a)) that is frequently used in the literature for these films [2,29–32]. The data obtained from the modelling are presented in Table 5. The R_{ct} values correlate with the corrosion rate results discussed before (section 3.2). The poorest corrosion performance is given for the films developed at pH 2.4, with the lowest charge transfer resistance values. At pH 2.9, this resistance increases, more markedly for the layers obtained in the

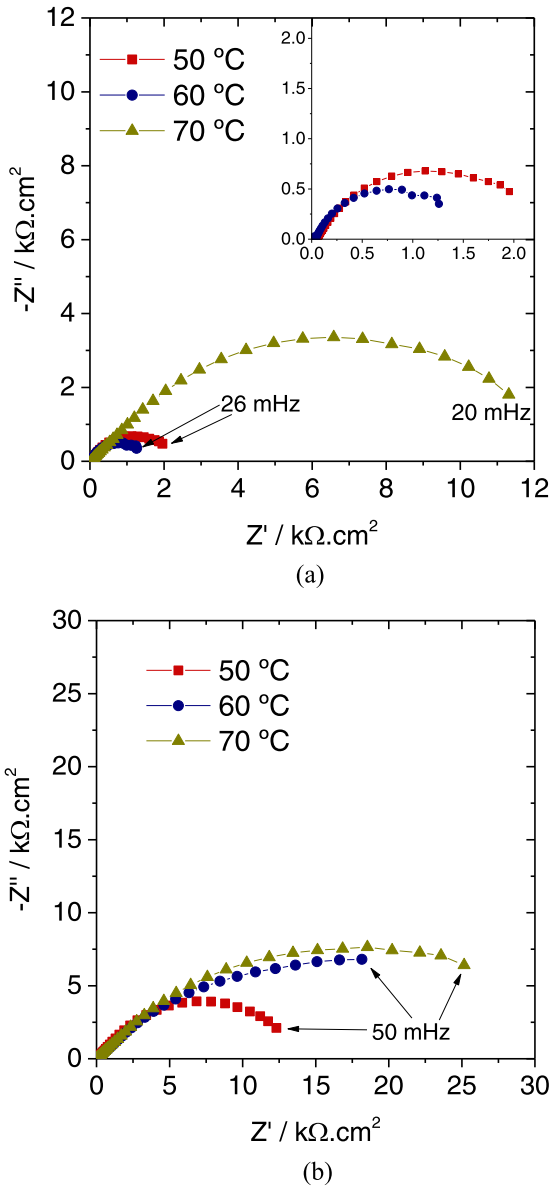

Fig. 4. Experimental Nyquist plots, recorded in 0.1 M Na_2SO_4 solution, of the phosphate layers developed at a) pH 2.4 and b) pH 2.9.

Table 5
Fitting data from the simulation with the equivalent circuit indicated in Fig. 1a of the impedance spectra presented in Fig 4.

	Temp.	R_{film} Ω. cm^2	C_{film} μF. cm^{-2}	R_{ct} Ω. cm^2	C_{dl} μF. cm^{-2}	CE%
pH 2.4	50 °C	32	25	2261	161	59
	60 °C	22	64	1473	415	>100
	70 °C	2356	13	10,537	14	12.7
pH 2.9	50 °C	1452	5	13,036	3	10.2
	60 °C	1366	0.7	38,323	8	3.5
	70 °C	1144	0.3	33,171	10	4

treatment performed at 60 and 70 °C. These layers had been previously discerned (Table 4) as those with the lowest current density values. When considering the R_{ct} value obtained for the bare substrate, an analogous estimation of the percentage of the uncovered area, as the data indicated in Table 4, can be deduced. The spectrum for the bare metal was modelled using the equivalent circuit presented in Fig. 1(a), with the difference that the portion related to the phosphate film was not included. The R_{ct} value of the uncovered metal was 1334.9 Ω·cm^2. The assessment of the coating efficiency, CE (expressed as uncovered area, %), can be obtained using as Eq. (3).

$$CE(\%) = \frac{R_{ct-unphosphated\ mteal}}{R_{ct-phosphated\ piece}} x100 \quad (3)$$

The poorest efficiency was evidenced for the layers developed in the bath at pH 2.4, with percentages of the uncovered area at 59% and >100% for the films prepared at 50 and 60 °C, respectively. On the contrary, the films developed at pH 3 achieved the best efficiency, where the percentage value of the uncovered area is reduced to 4% for the treatment performed at 70 °C.

According to the data included in Table 5, two coating classes could be discerned. Some coatings belong to the "poorer quality coating" class where a small value for the R_{film} and a high value for the C_{film} was obtained. The opposite is true for the "better quality coating" class. Then, the development of a more compact and denser layer for the second class, where the electrolyte has a more limited accessibility to the metal surface, could be concluded. However, when comparing the resistance and capacitance values in these two classes, one can visualize that the differences among the resistance values are more important than the differences among the capacitance values. This points that these differences are not uniquely derived from a geometrical factor. This mismatch is an indication that the circuit used for the modelling, although apparently suitable for the assessment of the coating efficiency, is not able to provide reliable information in the own coating characteristics.

Going again to the Nyquist plots, some curious feature can be discerned. Those coatings belonging to the poorest class (Fig.4(a)) show the conventional semicircle although a little flattened since the surface is not uniform, which produces a dispersion of the time constants [33]. For those coatings with an improved performance (Fig.4(b)), a straight line, at 45°, can be discerned, in the high frequency domain, followed by a skewed semicircle. This type of representation has been classically assigned to the response of a porous electrode where the electrical signal is not able to penetrate to the bottom of the pore [26,34]. Thus, the circuit, indicated in Fig.1(b), based on a transmission line was considered as a suitable candidate for the simulation of those layers priorly identified as the "better quality" class. The remaining layers should not be modelled using such a circuit since the graphical analysis of the Nyquist plots was not consistent with the formation of a porous electrode. Table 6 compiles the data obtained from the fitting with this model. A good correspondence between the experimental and the fitted data can be verified in Fig. 5.

The resistances attributed to the response of the uncovered areas, R_2, are comparable to the values referred to before (Table 5), so this model based on the TL provides an analogous coating efficiency. Therefore, this good correspondence could be used as an indication of the model's suitability.

Concerning the values of the time constant assigned to the interface of the electrode material with the electrolyte inside the pores, R_1 and C_1, significant differences can be identified among the capacitance values. However, the resistance values remain on a similar scale. Notably, the capacitance is smaller for the coatings obtained in the treatment at 60 and 70 °C and pH 2.9. Compared to the other films, the minor variation obtained for the resistance points to modifications in the film characteristics other than a geometrical factor. Whether the time constant value is computed, differences of the rate of the interaction at the electrode/electrolyte interface are revealed. Thus, the time constant is 65.5 s for the film obtained at pH 2.4 (70 °C), whereas the values for the layers obtained at pH 2.9 decreased to 10.5 s, 1.6 s and 0.8 seconds when formed at 50, 60 and 70 °C, respectively. Modifications in this time constant can be attributed to changes in the conductivity of the own electrode material, i.e., the phosphate film, since the testing electrolyte was the same for all the tested specimens. The shorter the time, the faster the interaction and, thus, the more conductive the material. The comparison among the R_m values agrees with this statement because this parameter decreases parallel to the reduction of the Z_1-time constant. The good correspondence between these parameters suggests the suitability of the TL model to provide information concerning the conduction ability of the phosphate films. A less acidic phosphating bath creates a more conductive layer. This property is still enhanced with the treatment's temperature increase. Thus, the phosphating solution's pH and temperature increment lead to the resulting film's higher conductive character.

Concerning the R_s parameter, the lowest value was developed for the layer prepared at pH 2.4. among the films obtained at pH 2.9, the increase in the temperature produced an increase in the value of this parameter. The R_s refers to the electrolyte inside the pores; no relevant variations should be obtained. The fact that these values do not correlate implies alterations in terms of the porous structure of the films. The R_s depends on the portion of the uncovered area and on the length of the phosphate layer according to Eq. (4).

$$R_s = R_{electrolyte}\frac{L_{pore}}{S_{uncovered}} \quad (4)$$

Unfortunately, the precise quantification of these parameters cannot be completed. About the uncovered area, the accurate value cannot be measured since it depends, as mentioned above, on the balance between the phosphate formation and the roughness increase at those sites. For the computation of the length, the coating mass was used and the formation of a film that grew normal to the metal surface was considered, in line with the sketch in Fig. 6a. However, the structure of the phosphate layer could be more complex, more tortuous, and then with longer effective pores, as represented in Fig. 6b.

Therefore, the variations in the R_s parameter reflect modifications produced due to changes in the uncoated area and the effective pore length. Both the increase in pH and the increase in temperature in the phosphating bath assist in developing films with a lower portion of the uncovered area or longer effective pores. Under these assumptions, an equivalent value for the resistivity of the electrolyte in the pores ($R_{electrolyte}$) would be obtained. More intricate and compact phosphate films are formed after treatment at high temperatures and pH. It is worth noting that the conversion coating formed at 70 °C and pH 2.9 exhibits a notable increase in the R_s parameter compared to the layer obtained at 60 °C and the same pH, although providing both a comparable coating efficiency (analogous R_2). Then, the increase in temperature at this pH is

Table 6
Fitting data obtained from the simulation with the equivalent circuit indicated in Fig. 1b of the impedance spectra presented in Fig. 4.

	Temp.	R_m kΩ.cm	R_s kΩ.cm	R_1 Ω.cm^3	C_1 mF.cm^{-3}	R_2 Ω.cm^2	C_2 μF.cm^{-2}
pH 2.4	70 °C	10530	72	117	565	13,356	20
pH 2.9	50 °C	111	407	125	85	15,369	17
	60 °C	23	5006	156	10	30,330	57
	70 °C	16	9579	97	8	35,663	24

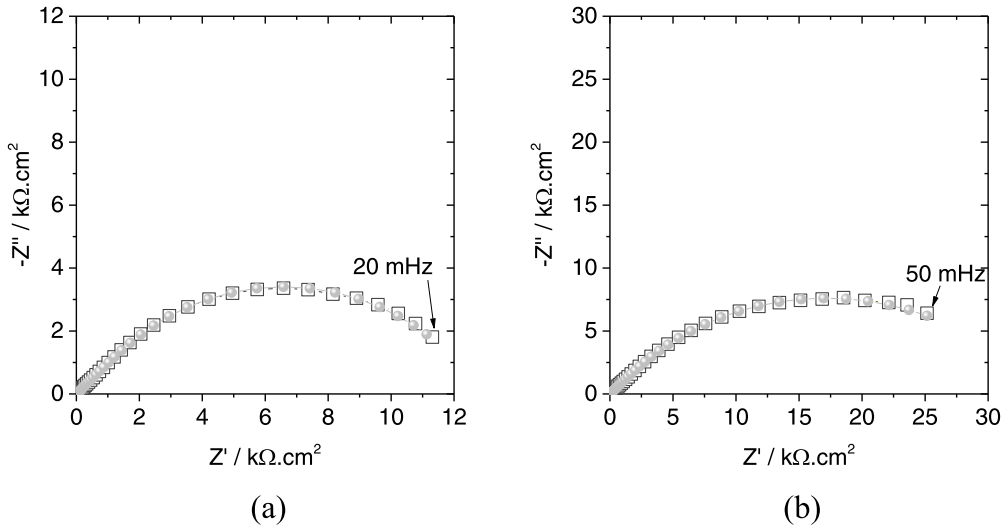

Fig. 5. Comparison of the experimental (hollow square) and fitted data (grey bubbles) (obtained with the transmission line model, Fig 1b) for the phosphate films prepared at 70 °C and a) pH 2.4 and b) pH 2.9.

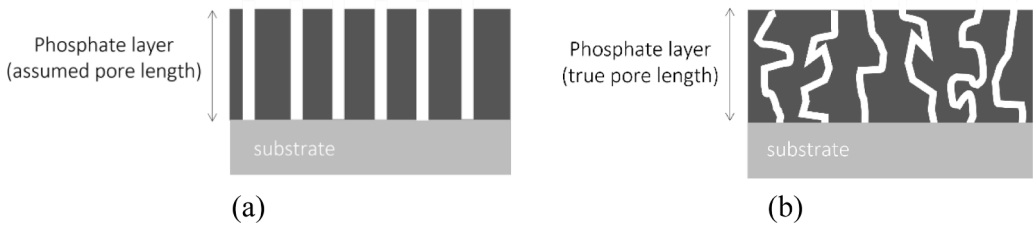

Fig. 6. Outline of the phosphate pore structure (white path): a) conventional approach and b) conceptual approach.

particularly helpful in creating a more complex pore structure.

4. Conclusions

The influence of pH and temperature in the phosphate conversion process was considered in this study. The phosphating bath used here was confirmed to be very sensitive to the changes in these parameters. At pH 2.4, the phosphoric pickling reaction is accelerated, but at 70 °C, the formation of the insoluble phosphate is also assisted so that the film can be rapidly constituted. At pH 2.9, an opposite condition was confirmed. The coating growth is slowed, and the nucleation of crystals controls the process. In addition, the increase in temperature does not markedly modify the resulting layer.

Microstructural and electrochemical techniques have been applied to characterise the phosphate films, which depend on the process variables. A film composed of smaller crystals, enriched in Fe, with a more intricate structure and able to cover more efficiently the metal surface is developed at pH 2.9, whereas at pH 2.4, thicker and less compact layers, with higher Zn content, are formed.

Any temperature or pH modification would require changes in the other substances added to the phosphating bath. Thus, for the bath used in this study, at pH 2.4 and 50 °C (or even 60 °C), the amount of phosphoric acid seemed to be excessive (since a complete coverage was not obtained), so that any corrective measure to decrease its content could be a possible improvement. At pH 2.4 and 70 °C, the bath shows pretty good performance, and even higher temperature values could be explored. At pH 2.9, the amount of phosphoric acid is too low, so the coating formation is too slow. The increase in temperature accelerates the reaction, but its effect is hardly relevant. The increase in the phosphoric acid content in this bath could be one possible adjustment to take benefit of this bath at this higher pH level. These suggested modifications will be explored in a future investigation.

CRediT authorship contribution statement

Sheila Silva-Fernández: Methodology, Validation, Formal analysis, Investigation, Resources. **Belén Díaz:** Conceptualization, Methodology, Writing – original draft, Writing – review & editing. **Iria Feijoo:** Formal analysis, Investigation. **Xosé Ramón Nóvoa:** Conceptualization, Methodology, Writing – review & editing, Project administration, Funding acquisition. **Carmen Pérez:** Conceptualization, Methodology, Writing – review & editing.

Declaration of Competing Interest

None.

Acknowledgments

The authors acknowledge grant # ED431B2021/14 from Xunta de Galicia Government. Funding for open access charge: Universidade de Vigo/CISUG.

References

[1] F. Simescu, H. Idrissi, Effect of zinc phosphate chemical conversion coating on corrosion behaviour of mild steel in alkaline medium: protection of rebars in reinforced concrete, Sci. Technol. Adv. Mater. 9 (2008), https://doi.org/10.1088/1468-6996/9/4/045009.

[2] J. Liu, B. Zhang, W.H. Qi, Y.G. Deng, R.D.K. Misra, Corrosion response of zinc phosphate conversion coating on steel fibers for concrete applications, J. Mater. Res. Technol. 9 (2020) 5912–5921, https://doi.org/10.1016/j.jmrt.2020.03.117.

[3] X. Zhao, R. Liu, W. Qi, Y. Yang, Corrosion resistance of concrete reinforced by zinc phosphate pretreated steel fiber in the presence of chloride ions, Materials 13 (2020), https://doi.org/10.3390/MA13163636 (Basel).

[4] B. Liu, X. Zhang, G.Y. Xiao, Y.P. Lu, Phosphate chemical conversion coatings on metallic substrates for biomedical application: a review, Mater. Sci. Eng. C 47 (2015) 97–104, https://doi.org/10.1016/j.msec.2014.11.038.
[5] M. Sheng, Y. Wang, Q. Zhong, H. Wu, Q. Zhou, H. Lin, The effects of nano-SiO_2 additive on the zinc phosphating of carbon steel, Surf. Coatings Technol. 205 (2011) 3455–3460, https://doi.org/10.1016/j.surfcoat.2010.12.011.
[6] S.M.A. Shibli, F. Chacko, Development of nano TiO_2-incorporated phosphate coatings on hot dip zinc surface for good paintability and corrosion resistance, Appl. Surf. Sci. 257 (2011) 3111–3117, https://doi.org/10.1016/j.apsusc.2010.10.125.
[7] N. Rezaee, M.M. Attar, B. Ramezanzadeh, Studying corrosion performance, microstructure and adhesion properties of a room temperature zinc phosphate conversion coating containing Mn^{2+} on mild steel, Surf. Coatings Technol. 236 (2013) 361–367, https://doi.org/10.1016/j.surfcoat.2013.10.014.
[8] B. Ramezanzadeh, H. Vakili, R. Amini, The effects of addition of poly(vinyl) alcohol (PVA) as a green corrosion inhibitor to the phosphate conversion coating on the anticorrosion and adhesion properties of the epoxy coating on the steel substrate, Appl. Surf. Sci. 327 (2015) 174–181, https://doi.org/10.1016/j.apsusc.2014.11.167.
[9] M. Tamilselvi, P. Kamaraj, M. Arthanareeswari, S. Devikala, J.A. Selvi, Development of nano SiO_2 incorporated nano zinc phosphate coatings on mild steel, Appl. Surf. Sci. 332 (2015) 12–21, https://doi.org/10.1016/j.apsusc.2015.01.177.
[10] R. Thomas, M.J. Umapathy, Nano silicon dioxide accelerated zinc phosphate conversion coating on mild steel using decyltriethylammonium bromide as an additive, Silicon 7 (2015) 371–381, https://doi.org/10.1007/s12633-014-9231-1.
[11] A.A. al-Swaidani, Modified zinc phosphate coatings: a promising approach to enhance the anti-corrosion properties of reinforcing steel, MOJ Civ. Eng. 3 (2017) 370–374, https://doi.org/10.15406/mojce.2017.03.00083.
[12] Y. Xie, M. Chen, D. Xie, L. Zhong, X. Zhang, A fast, low temperature zinc phosphate coating on steel accelerated by graphene oxide, Corros. Sci. 128 (2017) 1–8, https://doi.org/10.1016/j.corsci.2017.08.033.
[13] M. Arthanareeswari, P. Kamaraj, M. Tamilselvi, S. Devikala, A low temperature nano TiO_2 incorporated nano zinc phosphate coating on mild steel with enhanced corrosion resistance, Mater. Today Proc. 5 (2018) 9012–9025, https://doi.org/10.1016/j.matpr.2017.12.349.
[14] J.P. Popić, B.V. Jegdić, J.B. Bajat, D. Veljović, S.I. Stevanović, V.B. Mišković-Stanković, The effect of deposition temperature on the surface coverage and morphology of iron-phosphate coatings on low carbon steel, Appl. Surf. Sci. 257 (2011) 10855–10862, https://doi.org/10.1016/j.apsusc.2011.07.122.
[15] X. Zhang, G. yong Xiao, C. cong Jiang, B. Liu, N. bo Li, R. fu Zhu, Y. peng Lu, Influence of process parameters on microstructure and corrosion properties of hopeite coating on stainless steel, Corros. Sci. 94 (2015) 428–437, https://doi.org/10.1016/j.corsci.2015.02.021.
[16] V. Asadi, I. Danaee, H. Eskandari, The effect of immersion time and immersion temperature on the corrosion behavior of zinc phosphate conversion coatings on carbon steel, Mater. Res. 18 (2015) 706–713, https://doi.org/10.1590/1516-1439.343814.
[17] W. Zai, Y. Su, H.C. Man, J. Lian, G. Li, Effect of pH value and preparation temperature on the formation of magnesium phosphate conversion coatings on AZ31 magnesium alloy, Appl. Surf. Sci. 492 (2019) 314–327, https://doi.org/10.1016/j.apsusc.2019.05.309.
[18] K. Abdalla, A. Rahmat, A. Azizan, The effect of pH on zinc phosphate coating morphology and its corrosion resistance on mild steel, Adv. Mater. Res. 626 (2013) 569–574, https://doi.org/10.4028/www.scientific.net/AMR.626.569.
[19] X. Ding, L.F. Xue, X.C. Wang, K.H. Ding, S.L. Cui, Y.C. Sun, M. Sen Li, Influence of bath pH value on microstructure and corrosion resistance of phosphate chemical conversion coating on sintered Nd-Fe-B permanent magnets, J. Magn. Magn. Mater. 416 (2016) 247–255, https://doi.org/10.1016/j.jmmm.2016.04.048.
[20] Z. Chunyan, L. Shangju, Y. Baoxing, L. Xiaopeng, C. Xiao-Bo, Z. Tao, W. Fuhui, Ratio of total acidity to pH value of coating bath: a new strategy towards phosphate conversion coatings with optimized corrosion resistance for magnesium alloys, Corros. Sci. 150 (2019) 279–295, https://doi.org/10.1016/j.corsci.2019.01.046.
[21] W. Rausch, The Phosphating of Metals, Finishing Publications Ltd., 1990.
[22] Z. Panossian, Phosphating of steel for cold forming processes, in: Q.J. Wang, Y.W. Chung (Eds.), Encycl. Tribology, 2013. 10.1007/978-0-387-92897-5_1187.
[23] T.S.N.S. Narayanan, Surface pretreatment by phosphate conversion coatings - a review, Rev. Adv. Mater. Sci. 9 (2005) 130–177.
[24] M.F. Morks, Magnesium phosphate treatment for steel, Mater. Lett. 58 (2004) 3316–3319, https://doi.org/10.1016/j.matlet.2004.06.027.
[25] B. Díaz, L. Freire, M. Mojío, X.R. Nóvoa, Optimization of conversion coatings based on zinc phosphate on high strength steels, with enhanced barrier properties, J. Electroanal. Chem. 737 (2015) 174–183, https://doi.org/10.1016/j.jelechem.2014.06.035.
[26] D.M. Bastidas, Interpretation of impedance data for porous electrodes and diffusion processes, Corrosion 63 (2007) 515–521, https://doi.org/10.5006/1.3278402.
[27] S. Joiret, M. Keddam, X.R. Nóvoa, M.C. Pérez, C. Rangel, H. Takenouti, Use of EIS, ring-disk electrode, EQCM and Raman spectroscopy to study the film of oxides formed on iron in 1M NaOH, Cem. Concr. Compos. 24 (2002) 7–15, https://doi.org/10.1016/S0958-9465(01)00022-1.
[28] R.C. Zeng, X.X. Sun, Y.W. Song, F. Zhang, S.Q. Li, H.Z. Cui, E.H. Han, Influence of solution temperature on corrosion resistance of Zn-Ca phosphate conversion coating on biomedical Mg-Li-Ca alloys, Trans. Nonferrous Met. Soc. China 23 (2013) 3293–3299, https://doi.org/10.1016/S1003-6326(13)62866-6 (English Ed.
[29] R. Ramanauskas, O. Girčienė, L. Gudavičiutė, A. Selskis, The interaction of phosphate coatings on a carbon steel surface with a sodium nitrite and silicate solution, Appl. Surf. Sci. 327 (2015) 131–139, https://doi.org/10.1016/j.apsusc.2014.11.120.
[30] C. Jiang, X. Cheng, Anti-corrosion zinc phosphate coating on building steel via a facile one-step brushing method, Electrochem. Commun. 109 (2019), 106596, https://doi.org/10.1016/j.elecom.2019.106596.
[31] S.R. Arunima, M.J. Deepa, L. Elias, T.R. Aju Thara, C.V. Geethanjali, S.M.A. Shibli, Tuning of surface characteristics of composite (WO_3/$BiVO_4$) zinc phosphate coatings for industrial applications, Appl. Surf. Sci. 543 (2021), 148822, https://doi.org/10.1016/j.apsusc.2020.148822.
[32] G. Xiaoyan, J. Huili, Corrosion resistance of zinc phosphated HRB400 steel in simulated concrete pore solution, Int. J. Electrochem. Sci. (2022) 17, https://doi.org/10.20964/2022.06.39.
[33] B. Hirschorn, M.E. Orazem, B. Tribollet, V. Vivier, I. Frateur, M. Musiani, Determination of effective capacitance and film thickness from constant-phase-element parameters, Electrochim. Acta 55 (2010) 6218–6227, https://doi.org/10.1016/j.electacta.2009.10.065.
[34] A. Lasia, Impedance of porous electrodes, J. Electroanal. Chem. 397 (1995) 27–33, https://doi.org/10.1016/0022-0728(95)04177-5.